Semicrystalline Lamellar Phase in Binary Mixtures of Very Long Chain *n*-Alkanes[1]

X. B. Zeng and G. Ungar*

Department of Engineering Materials, University of Sheffield, Sheffield S1 3JD, U.K.

Received May 15, 2001; Revised Manuscript Received July 14, 2001

ABSTRACT: Lamellar structure formed by melt crystallization of binary mixtures of monodisperse long *n*-alkanes $C_{122}H_{246}$, $C_{162}H_{326}$, $C_{194}H_{390}$, $C_{210}H_{422}$, $C_{246}H_{494}$, $C_{258}H_{518}$, and $C_{294}H_{590}$ was studied by small-angle X-ray scattering (SAXS) and thermal analysis. A semicrystalline form (SCF) was found to be the stable phase over a wide range of compositions in the temperature range between the melting points of the shorter alkane and that of the alkane with a length equal to the difference between the chain lengths of the two components. Lamellar structure of SCF is determined by Fourier synthesis of electron density profiles from SAXS intensities and by fitting to models. It was found that SCF consists of alternating crystalline and amorphous layers. The thickness of crystalline layers is defined by the extended chain length of the shorter alkane tilted at 35° to the layer normal. The shorter chains are fully crystalline and confined to the crystal layers. The longer molecules traverse the crystal layer and are only partially crystalline; their surplus length in the form of loose cilia makes up the amorphous layer. The structure is similar to the transient noninteger folded (NIF) form in pure long *n*-alkanes. Stable SCF solid solution was found in alkanes with length ratio up to 1.7:1 and a chain length difference of up to 100 carbons, having a crystallinity as low as 63%. Viability of a stable SCF is demonstrated by a simple thermodynamic calculation based on the above structural model. According to the $C_{162}H_{326}-C_{246}H_{494}$ phase diagram, the maximum molar fraction of $C_{246}H_{494}$ that SCF will accept is 0.44. Taking into account the 35° chain tilt, this means that the effective cross-sectional area of a chain crossing the crystalline−amorphous interface increases by a factor of 2.8.

1. Introduction

Since pure normal alkanes C_mH_{2m+2} with m between 100 and 400 were first synthesized[2−4] their crystallization and lamellar structure in the solid state were studied in some detail. It was found that in the stable crystalline phase, as in the case of shorter chain analogues,[5−7] alkane molecules are extended and packed into layers. However, contrary to paraffins with m up to 40−50, each layer in very long alkanes acts as a separate crystal; i.e., there is no evidence of crystallographic register between layers. In addition to the most stable extended-chain form, with increasing chain length an increasing number of metastable lamellar forms can be obtained in very long paraffins, having folded chains. There is preference for a chain traverse through the crystal layer to be an integer fractions of the full chain, e.g., 1, $^1/_2$, $^1/_3$, resulting in "integer-folded" forms.[8−10]

It was found further that in the early stages of melt crystallization a "noninteger folded" (NIF) form appears.[11] Its layer periodicity, as determined by small-angle X-ray scattering (SAXS), does not correspond to an integer fraction of the molecular length. NIF is a transient semicrystalline form less stable than the integer forms with comparable periodicities. It can transform to these forms via lamellar thickening or thinning in the solid state.[11,12] Lamellar structure of NIF has been determined recently by a detailed SAXS study,[12] and it will be referred to later in the Discussion.

In the present paper, we turn to binary mixtures of long *n*-alkanes. Studies of mixtures with controlled polydispersity are expected to contribute to a better understanding of crystallization and morphology of polymers. Furthermore, such studies are of interest as an extension of the active research on shorter alkanes where notable developments have taken place recently, particularly in the area of mixtures.[13−21] The interest in shorter alkanes is driven by their connection with waxes, lipids, Langmuir−Blodgett films, liquid crystals, etc.

It had been thought originally that binary mixtures of short paraffins do not form solid solutions unless the chain lengths differed by less than three to four carbon atoms.[22−32] However, more recently new modes of cocrystallization have been suggested for mixtures of alkanes which differ by four to ten carbon atoms.[13,14,17,19,20] The common feature of these mixing modes are varying degrees of microphase separation into adjacent molecular layers. However, large discrepancies in chain lengths are not tolerated by crystals of shorter alkanes, as shown, e.g., by phase separation between $C_{28}H_{58}$ and $C_{44}H_{90}$ in the solid.[13] Smith and Manley studied quasi-binary systems of polyethylene fractions with molecular weights ($\bar{M}_n$): (1) 980 and 1790 (equivalent to $C_{70}H_{142}$ and $C_{128}H_{258}$), and (2) 1790 and 20×10^3.[33] They found that fractionation occurs during the crystallization process at cooling rates lower than 20 °C/min. Solid solutions were only found upon quenching to temperatures lower than 80 °C.

In this paper, we report the results of the first structural and thermodynamic study of binary mixtures of very long chain *n*-alkanes. Series of binary mixtures of *n*-alkanes differing by tens to more than 100 CH_2 groups were studied. A novel mode of cocrystallization of widely disparate paraffins is described, termed semicrystalline form (SCF). We report first on its lamellar structure as determined by SAXS. Next we construct the phase diagram of a representative binary system, $C_{162}H_{326} + C_{246}H_{494}$, and show the semicrystalline form to be the stable phase over a sizable range of compositions and temperatures. Finally, the thermodynamics

10.1021/ma010853r CCC: $20.00
Published on Web 08/30/2001

of the SCF is discussed in order to explain its stability over the phase separated extended chain forms.

2. Experimental Section

2.1. Materials. The pure long chain *n*-alkanes used in this work were kindly provided by Drs. G. M. Brooke and S. Mohammed, University of Durham. For details on the synthesis see ref 34. The alkanes used in this work are $C_{122}H_{246}$, $C_{162}H_{326}$, $C_{194}H_{390}$, $C_{210}H_{422}$, $C_{246}H_{494}$, $C_{258}H_{518}$, and $C_{294}H_{590}$. Mixtures, in small glass test tubes, were melted repeatedly for several minutes under nitrogen followed by quench-crystallization, to ensure homogeneous mixing.

2.2. Small-Angle X-ray Scattering (SAXS). The in situ SAXS experiments were performed on Station 8.2 of the Daresbury Synchrotron Radiation Source. The beam was mononchromatized to $\lambda = 1.5$ Å and double-focused onto the detector, with a cross section of 1 × 0.3 mm in the sample plane.[35] A high count rate quadrant multiwire detector was used, and the sample to detector distance was 3.1m. The capillary with the sample was held in a Linkam hot stage with temperature control within 0.2 °C. The beam was monitored with two ionization chambers. All diffractograms were corrected for uneven channel response by dividing them with the response to homogeneous radiation of ^{55}Fe. The correction for positional nonlinearity of the detector was done using the first 22 orders of diffraction from wet rat tail collagen. Two third-order polynomials, linked by matching their boundary values of zeroth and first derivatives, were fitted to the inverse collagen spacings for each half of the detector range. A separate linearization function was applied for each experimental session. The sample-to-detector distance was calibrated using polycrystalline samples of shorter orthorhombic *n*-alkanes with precisely known unit cell lengths.

2.3. Differential Scanning Calorimetry (DSC). DSC experiments were performed on a Perkin-Elmer Pyris-1 instrument. Samples were sealed in 10 mm aluminum DSC pans, and the sample amount was around 1 mg. When determining the phase diagram, the heating rates were normally 2 °C/min. Temperatures and enthalpies were calibrated by indium. Temperature correction for isothermal and cooling cycles was derived by extrapolation using different heating rates. Peak temperatures were corrected for thermal resistance.[36]

3. Results

3.1. SAXS of the High Temperature Form. 3.1.1. Experimental Diffractograms. Figure 1 shows a typical series of SAXS traces of a binary mixture of long alkanes, in this case 1:1 w/w $C_{162}H_{326}$ + $C_{246}H_{494}$, recorded during cooling from the melt (a) and subsequent heating (b). A series of Bragg diffraction peaks arise from regular stacking of molecular layers. Crystallization (melting) takes place at 120 °C (131 °C), and a clear transition occurs at 95 °C (105 °C) during cooling (heating). Wide-angle scattering (WAXS) recorded simultaneously shows the crystal unit cell to be the orthorhombic *Pnam*, as in polyethylene,[37] and this remains unchanged in the transition. The series of SAXS curves recorded during the heating cycle (Figure 1b) is almost an exact replica of Figure 1a, showing that the transition is reversible with a hysteresis of ca. 10 °C.

The small-angle diffractogram of the high-temperature phase consists of a series of Bragg-like diffraction orders of a single periodicity *L*. In the case of the 1:1 w/w mixture of $C_{162}H_{326}$ + $C_{246}H_{494}$ *L* is 215 Å (measured at 114 °C in the heating cycle—Figure 1b). This spacing falls between the values for extended chain forms of pure $C_{246}H_{494}$ (258 Å) and $C_{162}H_{326}$ (170 Å) crystallized form melt. Measured *L* using the Bragg equation increases somewhat with increasing temperature (225 Å at 130 °C, i.e., just below the melting point). When the mixture is held in the high-temperature form for many hours, there is no evidence of change in either the position or intensity of the diffraction peaks. The fact that *L* is intermediate between the values for the pure components suggests a solid solution.

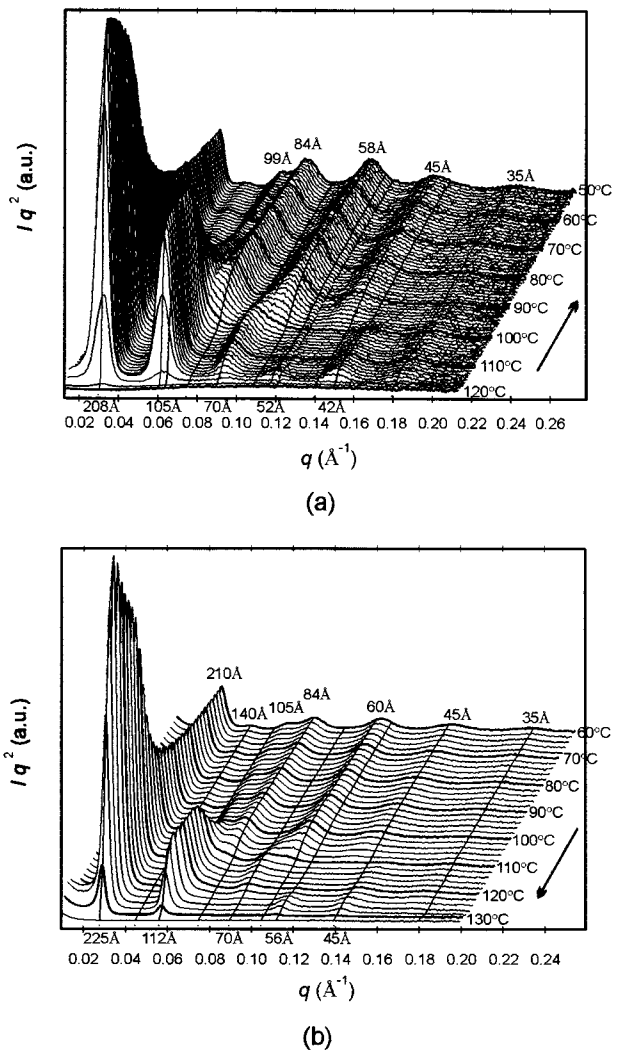

Figure 1. Small-angle X-ray scattering spectra recorded during cooling (a) and heating (b) of a binary mixture of $C_{162}H_{326}$ and $C_{246}H_{494}$(1:1 by weight, 3:2 molar). The respective cooling and heating rates were 2 and 5 °C/min. Intensities are Lorentz corrected. Constant *q* lines are labeled by the corresponding Bragg spacings (in Å).

The diffraction peaks of the high-temperature phase are sharp which suggests a good stacking order of the lamellae. The line widths of the diffraction peaks are 8.5×10^{-4} rad, and that of the resolution function, measured from the central beam by using a semitransparent beam stop, is 3.3×10^{-4} rad. The correlation length $\xi = \lambda/\Delta$ is thus calculated to be 3×10^3Å, an equivalent of about 15 stacked lamellae.

The low temperature form (or forms) has a more complicated SAXS pattern. The peaks are broader, which is common in phases formed through solid-state transformation, and indexing is not straightforward. The current paper deals with the high-temperature phase only, while the more complex low-temperature phase is treated elsewhere.[1,38]

The phase sequence melt → high-*T* form → low-*T* form(s) upon cooling and its reverse upon heating

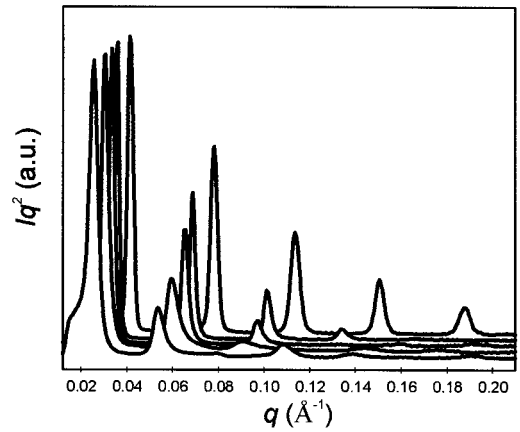

Figure 2. SAXS diffractograms for different melt-crystallized binary mixtures of $C_{162}H_{326}$+ X recorded at temperatures 10−15 °C below the melting point. From top to bottom: pure $C_{162}H_{326}$, $C_{162}H_{326}$ + $C_{194}H_{390}$, $C_{162}H_{326}$ + $C_{210}H_{422}$, $C_{162}H_{326}$ + $C_{246}H_{494}$, and $C_{162}H_{326}$ + $C_{258}H_{518}$. Except for the pure $C_{162}H_{326}$, the mixtures are 1:1 by weight. Intensities are normalized to that of the first-order peak.

prevails in the binary mixtures studied. Small-angle diffractograms of the high-temperature form for a series of binary mixtures with $C_{162}H_{326}$ as the shorter chain component are shown in Figure 2. As the chain length of the longer component increases, so does the lamellar spacing, but in all cases the periodicity is intermediate between those of the pure components.

Summarized, the following are the common features of the high-temperature form immediately apparent from the SAXS patterns:

1. SAXS consists of a series of sharp diffraction peaks which can be indexed as orders of a fundamental periodicity L and attributed to a lamellar structure.

2. L lies between the values for the extended forms of the two constituent components and does not change significantly with temperature or annealing time.

3. The larger the difference between molecular lengths of the two components, the steeper is the descent of intensity with increasing diffraction order. In many cases (e.g., 1:1 w/w mixtures of $C_{162}H_{326}$ + $C_{246}H_{494}$ and $C_{162}H_{326}$ + $C_{258}H_{518}$ in Figure 2) the intensities pass through a minimum with increasing diffraction order.

4. For binary mixtures with longer/shorter weight ratio less than 50:50 this high-temperature form is the only phase presents close to the melting point of the mixture and is stable.

The information contained in the positions and intensities of the SAXS peaks can be used to Fourier reconstruct the one-dimensional projection of electron density and hence obtain an insight into the structure of the high-temperature form.

3.1.2. Reconstruction of Electron Density Profiles.[12] The small-angle X-ray diffraction from stacks of lamellae which are large compared to the stacking period is related to the one-dimensional electron density profile normal to the stacks $E(x)$ by Fourier transformation. As $E(x)$ is periodic and normally centrosymmetric, its corresponding diffraction amplitude A_n can be expressed as

$$A_0 = \frac{1}{L}\int_0^L E(x)\,\mathrm{d}x \tag{1a}$$

$$A_n = \frac{2}{L}\int_0^L E(x)\cos\left(\frac{2\pi nx}{L}\right)\mathrm{d}x, \quad n > 0 \tag{1b}$$

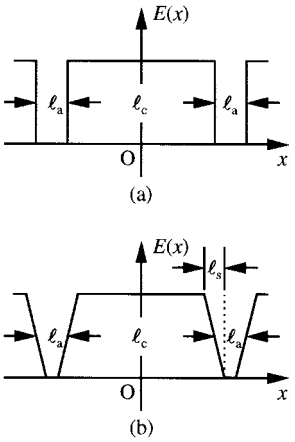

Figure 3. Model electron density profiles used for fitting to the experimental SAXS data: (a) model I (rectangular); (b) model II (trapezoidal). x axis is normal to layers.

Here L is the periodicity normal to the lamellae. Conversely, $E(x)$ can be expressed by A_n as

$$E(x) = \sum_{n=0}^{\infty} A_n \cos\left(\frac{2\pi nx}{L}\right) \tag{2a}$$

or if using only the first N terms, we define:

$$E_N(x) = \sum_{n=0}^{N} A_n \cos\left(\frac{2\pi nx}{L}\right) \tag{2b}$$

Experimentally we measure the intensity of the nth diffraction peak I_n which is equal to A_n^2, and its wave vector q_n which is equal to $2\pi n/L$. Ideally

$$E(x) = \sum_{n=0}^{\infty} \sqrt{I_n}\cos(q_n x + \phi_n), \quad \phi_n = 0, \pi \tag{3a}$$

Since it is impossible to measure an infinite number of diffraction orders, an approximation can be achieved with first N orders:

$$E(x) \approx E_{exp}(x) = \sum_{n=0}^{N} \sqrt{I_n}\cos(q_n x + \phi_n), \quad \phi_n = 0,\pi \tag{3b}$$

The phase of the structure factor, represented by ϕ, can be determined with a high degree of confidence in the present case by trial and error, considering reasonable physical models and their variation with changing alkane chain length and composition. The electron density profile can be directly reconstructed from the diffraction pattern via eq 3b. An example profile $E_{exp}(x)$ for a 1:1 w/w mixture of $C_{162}H_{326}$ + $C_{246}H_{494}$ is shown in Figure 4 (dots); intensities of $N = 6$ diffraction orders are taken into account.

3.1.3. Model Density Profiles. In this study, we use eq 1 to calculate the diffraction pattern of different theoretical model electron density profiles and fit them to the experimental diffractogram. Here the choice of models has been narrowed down to two. The first is a simple rectangular periodic wave (Figure 3a) with alternating regions of high and low electron density. It will be shown below that good agreement with independently measured degree of crystallinity is achieved if these regions are associated with crystalline and amorphous sublayers. The thicknesses of the two sublayers, ℓ_c and ℓ_a, are adjustable parameters in the fitting to the experimental diffraction data, with $\ell_c + \ell_a = L$.

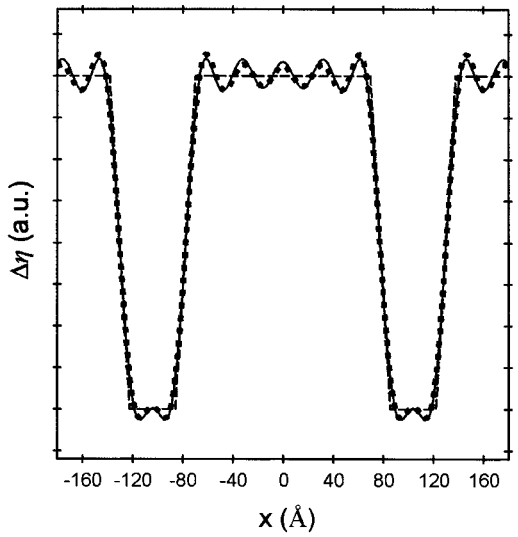

Figure 4. Comparison of reconstructed electron density profiles for the 1:1 w/w $C_{162}H_{326} + C_{246}H_{494}$ binary mixture and the best-fit model: (■) $E_{exp}(x)$, reconstructed from experimental data for $N = 6$ diffraction orders, phase sign sequence $+-++-+$ is used; (−) $E_N(x)$, reconstruction from model II using $N = 6$ Fourier terms; (- -) best-fit model.

The electron density projection $E_I(x)$ for the rectangular model can be expressed as

$$E_I(x) = \begin{cases} E_0 & nL - \ell_c/2 < x < nL + \ell_c/2 \\ 0 & \text{for other } x \end{cases} \quad (4)$$

A modified model $E_{II}(x)$, the "trapezoidal model", is also tested, having a transition layer of thickness ℓ_s with a linear density gradient (Figure 3b). It is described by

$$E_{II}(x) = \begin{cases} E_0 & (-\ell_c + \ell_s)/2 < x < (\ell_c - \ell_s)/2 \\ E_0(x + (\ell_c + \ell_s)/2)/\ell_s & (-\ell_c - \ell_s)/2 < x < (-\ell_c + \ell_s)/2 \\ E_0((\ell_c + \ell_s)/2 - x)/\ell_s & (\ell_c - \ell_s)/2 < x < (\ell_c + \ell_s)/2 \\ 0 & \text{for other } x \end{cases} \quad (5)$$

The parameters used are all marked in Figure 3.

Figure 4 illustrates the match between the "experimental" electron density profile $E_{exp}(x)$ (dots) and that calculated, $E_N(x)$ (solid wavy line), for the best fitting model. In the calculation of $E_N(x)$ the same number, $N = 6$, of Fourier terms were used as the number of diffraction orders taken into account in the determination of $E_{exp}(x)$. The reconstruction is for 1:1 w/w $C_{162}H_{326} + C_{246}H_{494}$ binary mixture. The model used is trapezoidal and is also shown in Figure 4 (broken straight lines). It is clear that the ripples in $E_{exp}(x)$ are artifacts due to the truncation of the Fourier series.

The best-fit trapezoidal model which represents the electron density distribution along the layer normal shows two distinct regions with different electron densities. Both models (rectangular and trapezoidal) can be used to fit the diffraction data. The measured intensities and those calculated from both models I and II, along with the parameters and R values, are listed in Table 1. It is clear that, although the use of model II (trapezoidal) gives a somewhat better fit, the difference in parameters ℓ_c and ℓ_a are almost negligible. Model profile II can be regarded as smeared profile I. The smearing may be either a genuine interphase effect or the result of averaging over imperfect layer stacking analogous to the way thermal disorder is accounted for by the Debye−Waller factor.[12] For simplicity model I is being used henceforth.

3.1.4. Structure of the High-Temperature Form. The best fitting rectangular models for the high-temperature form for all 1:1 (w/w) $C_{162}H_{326} + X$ mixtures shown in Figure 2, as well as for the extended chain form of pure $C_{162}H_{326}$, have been calculated and are shown in the form of a histogram in Figure 5a. It is evident that in these models one sublayer of the lamella (assuming to be the part with high electron density) has almost constant thickness ℓ_c, unaffected by the chain length of the X component. At the same time the other sublayer (assuming to have a lower electron density) changes from mixture to mixture: the longer the chains of component X the greater the thickness ℓ_a of the sublayer. In the case of the extended chain form of pure $C_{162}H_{326}$ there is little doubt that, of the two sublayers, it is the one with 156 Å thickness which corresponds to the crystalline core of the lamella, while the 14 Å thick sublayer has the lower electron density and corresponds to the less ordered lamellar surface.[12] Thus, it is suggested that, in the binary mixtures, the assumed high electron density sublayer corresponds to the crystalline core of the lamella, while the low electron density sublayer is less ordered or even amorphous.

The amorphous nature of the low electron density sublayer is supported by independent measurement of crystallinity of the 1:1 w/w mixture of $C_{162}H_{326}$ and $C_{246}H_{494}$ using WAXS and DSC. The WAXS crystallinity of this sample in the SCF is only 79%, the mixture having been slowly cooled from melt (0.5 °C/min) and subsequently annealed at 114 °C. The corresponding melting enthalpy of the SCF, measured by DSC, is only 236 J/g which is equivalent to a crystallinity of 81% (293 J/*g* is the heat of fusion of fully crystalline polyethylene). These results match reasonably well the $\ell_c/(\ell_c + \ell_a)$ value of 75% (equivalent to a weight crystallinity of 78%) for the best-fit rectangular model as derived from the SAXS experiment. We note that, in accordance with the model below, $^5/_6$ or 83 wt % of the material is expected to be crystalline in a 1:1 w/w mixture of $C_{162}H_{326}$ and $C_{246}H_{494}$, assuming that only the surplus chain length of alkane $C_{246}H_{494}$ is amorphous.

This leads us to propose a lamellar structure model for the high temperature forms as drawn in Figure 6a. Molecules of the shorter of the two alkanes crystallize fully and set the thickness of the crystalline layer. The longer molecules traverse the crystalline layer, but their protruding surplus length, or cilia, remains amorphous thus creating the amorphous sublayer. The structure is thus intrinsically semicrystalline, even though the individual components are fully crystallizable. The semicrystalline form (SCF) exists below the melting points of the shorter component. However it may also exist somewhat above the melting point of the shorter component; in the $C_{122}H_{246} + C_{162}H_{326}$ 25:75 w/w mixture it has been observed to form at 121.0 °C, 1.8 °C above T_m of $C_{122}H_{246}$ (119.2 °C).

Thus far we have examined binary mixtures with $C_{162}H_{326}$ as the shorter component. Results of electron density reconstruction for other mixtures are plotted in Figure 5, parts b and c. We can see that the $C_{194}H_{390} + X$ series (1:1 w/w) behave in the same way as the $C_{162}H_{326} + X$ series: ℓ_c is almost exactly the same as in pure $C_{194}H_{390}$, and ℓ_a increases with the molecular length of the longer alkane component.

Table 1. Best-Fit Parameters, Diffraction Intensities and *R* Values for Semicrystalline Form in Different Alkane Mixtures[a]

		parameters (Å)				diffraction intensities (a.u.)							
sample	results	L	ℓ_c	ℓ_a	ℓ_s	1	2	3	4	5	6	7	R
$C_{162}+C_{258}$	expt	235				10.78	2.05	0.07	0.84	0.22	0.08	0.09	
1:1 w/w	model I	235	152.4	82.6		10.49	2.13	0.04	0.75	0.25	0.04	0.27	0.068
at 130 °C	model II	235	152.3	82.7	14.8	10.89	2.11	0.04	0.64	0.19	0.03	0.14	0.051
$C_{162}+C_{246}$	expt	215				13.21	5.95	1.09	0.00	0.27	0.40		
1:1 w/w	model I	215	155.6	59.4		12.29	6.07	1.32	0.00	0.51	0.67		0.069
at 120 °C	model II	215	155.7	59.3	16.1	12.88	6.01	1.17	0.00	0.33	0.34		0.021
$C_{162}+C_{210}$	expt	200				5.12	2.56	0.67	0.01	0.06	0.13		
1:1 w/w	model I	200	152.7	47.3		4.77	2.59	0.72	0.02	0.12	0.27		0.072
at 120 °C	model II	200	152.6	47.4	16.7	5.11	2.58	0.64	0.01	0.07	0.12		0.011
$C_{162}+C_{194}$	expt	193				6.55	4.15	1.87	0.48	0.04			
1:1 w/w	model I	193	155.9	37.1		6.26	4.24	2.03	0.54	0.01			0.038
at 120 °C	model II	193	158.4	34.6	20.3	6.54	4.18	1.86	0.48	0.04			0.002
C_{162}	expt	170				1.47	1.42	1.18	0.95	0.87			
at room temp	model I	170	155.9	14.1		1.46	1.36	1.21	1.03	0.82			0.023
	model II	170	158.4	11.6	8.5	1.47	1.37	1.21	1.02	0.82			0.021
$C_{194}+C_{294}$	expt	240				5.63	2.59	0.38	0.00	0.09	0.17	0.09	
1:1 w/w	model I	240	179.1	60.9		5.21	2.54	0.53	0.00	0.23	0.28	0.09	0.086
at 123 °C													
$C_{194}+C_{246}$	expt	236				1.62	0.68	0.30	0.06				
1:1 w/w	model I	236	184.8	51.2		1.43	0.86	0.32	0.04				0.084
at 115 °C													
$C_{194}+C_{210}$	expt	214				4.16	3.33	2.20	1.31	0.67	0.33	0.18	
1:1 w/w	model I	214	187.1	26.9		3.73	3.17	2.40	1.57	0.85	0.34	0.07	0.074
at 125 °C													
C_{194}	expt	203				6.99	6.12	5.64	4.94	4.52	3.37		
at room temp	model I	203	188.1	14.9		6.68	6.33	5.78	5.08	4.27	3.43		0.018
$C_{162}+C_{246}$	expt	204				1.91	0.03	0.13	0.03				
1:9 w/w	model I	204	111	93		1.86	0.04	0.18	0.03				0.049
at 120 °C													
$C_{122}+C_{246}$	expt	195				13.22	0.40	0.83	0.32				
1:1 w/w	model I	195	108.9	86.1		12.86	0.43	1.07	0.37				0.037
at 124 °C													
$C_{122}+C_{210}$	expt	187				13.00	1.1	0.17	0.69				
1:1.7 w/w	model I	187	116.3	70.7		10.60	1.5	0.23	0.77				0.104
at 120 °C													
$C_{122}+C_{162}$	expt	155				3.39	2.09	0.83	0.20	0.02	0.00		
3:2 w/w	model I	155	125.9	29.1		3.00	2.07	1.03	0.30	0.01	0.04		0.098
at 105 °C													
C_{122}	expt	129				14.46	13.01	10.97	7.24				
at room temp	model I	129	114.3	14.7		14.73	12.92	10.37	7.48				0.016

[a] $R = (\Sigma_n(|A_{n,\mathrm{exp}}| - |A_{n,\mathrm{mod}}|)^2/\Sigma_n|A_{n,\mathrm{exp}}|^2)^{1/2}$.

Turning to the $C_{122}H_{246}$ + X series, we note that in the case of the mixture $C_{122}H_{246}$ + $C_{162}H_{326}$ (3:2 w/w) ℓ_c is equal to 126 Å, somewhat higher than the value for pure $C_{122}H_{246}$ (114 Å); however, the basic semicrystalline lamellar structure is still the same as in the systems described above. The larger ℓ_c value for this mixture may be due to a smaller tilt angle of the chains: instead of the usual 35° tilt, which corresponds to the basal planes being {201}, the tilt here is only 22°. This is close to 19°, the value corresponding to {101} basal planes, commonly observed in shorter alkanes. In the mixture $C_{122}H_{246}$ + $C_{210}H_{422}$ (1:1 molar, 37:63 w/w) ℓ_c is 117 Å, very close to that of pure $C_{122}H_{246}$. The crystallinity of this latter mixture is only 63%, which is so far the lowest found in the stable SCF.

In the $C_{122}H_{246}$ + $C_{246}H_{494}$ mixture, the ratio of chain lengths is practically 1:2 and the chain length difference of 124 methylene groups is the largest in this study. In the 1:1 and 1:3 w/w mixtures, the semicrystalline phase is not stable, and it transforms rapidly and continuously into a fully crystalline form, which appears to consist of folded chains of $C_{246}H_{494}$ and extended chains of both $C_{246}H_{494}$ and $C_{122}H_{246}$.[38,42]

Added to Figure 5c is the 1:9 w/w mixture $C_{162}H_{326}$ + $C_{246}H_{494}$, which will be commented on further below.

To confirm the validity of our structural model, we have also investigated changes in the semicrystalline form with changing composition for a given binary system. The fitting results for SCF in a series of $C_{162}H_{326}$ + $C_{246}H_{494}$ mixtures are shown in Figure 7. It is clear that for most compositions the crystalline layer adopts the same thickness as in pure $C_{162}H_{326}$. With increasing proportion of $C_{246}H_{494}$, ℓ_a increases, with a consequent increase in L. This behavior is to be expected since more protruding cilia are introduced, resulting in an increasing amorphous fraction.

The exception to the above trend in the $C_{162}H_{326}$ + $C_{246}H_{494}$ mixtures is the case of the 1:9 w/w blend. Here, as in pure $C_{246}H_{494}$ cooled from melt at a rate ≥1 °C/min,[39] the $C_{246}H_{494}$ chains adopt the once-folded conformation rather than the extended one, even at cooling rate 1 or 2 orders of magnitude lower than in pure $C_{246}H_{494}$. The reason for chains above a certain length to fold[8] is that thinner lamellar crystals grow faster, a well-established fact in polymers.[40,41] The molecules of $C_{246}H_{494}$ fold nearly exactly in the middle,[8,12,42] and it is the shorter stem length corresponding to 246/2 = 123 C atoms which sets the value of ℓ_c here, rather than the length of the extended chains of $C_{162}H_{326}$—see Figure 6b. The parameters of the 1:9 $C_{162}H_{326}$ + $C_{246}H_{494}$ mixture are also included in Figure 5c for comparison with the $C_{122}H_{246}$ + X mixtures; the ℓ_c value for the 1:9 $C_{162}H_{326}$ + $C_{246}H_{494}$ mixture is identical to those for the $C_{122}H_{246}$ + X series, within the experimental error. The

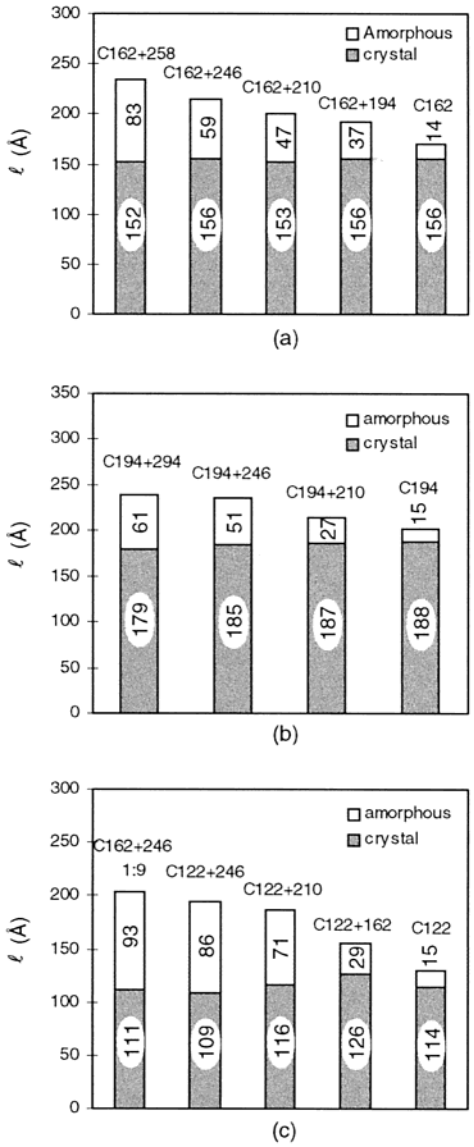

Figure 5. Comparison of best-fit parameters ℓ_c and ℓ_a and $L = \ell_c + \ell_a$ for the rectangular electron density model of the semicrystalline form for the binary series: (a) $C_{162}H_{326}$ + X, (b) $C_{194}H_{390}$ + X, and (c) $C_{122}H_{246}$ + X. Weight ratio of components is 1:1 unless specified otherwise. Also included in part c is the 1:9 mixture of $C_{162}H_{326}$ + $C_{246}H_{494}$ in which $C_{246}H_{494}$ chains are folded in two; hence, ℓ_c is the same as in the $C_{122}H_{246}$ + X series.

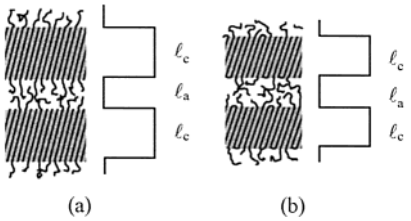

Figure 6. Schematic representation of molecular arrangement in semicrystalline forms of binary mixtures of long chain *n*-alkanes: (a) stable SCF, crystalline layer thickness is determined by the length of extended chains of shorter molecules; (b) metastable SCF, crystalline layer thickness is determined by the fold length of once-folded chains of longer molecules (as in the case of $C_{162}H_{326}$ + $C_{246}H_{494}$, 1:9 mixture).

folded-chain semicrystalline form in the 1:9 $C_{162}H_{326}$ + $C_{246}H_{494}$ mixture is metastable and extended-chain $C_{246}H_{494}$ separates out after prolonged annealing.

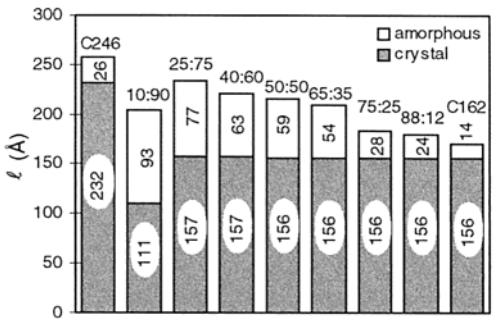

Figure 7. Comparison of best-fit model parameters for SCF in $C_{162}H_{326}$ + $C_{246}H_{494}$ mixtures of different compositions. The parameters for the 25:75 w/w mixture are for an early stage of crystallization, before the appearance of extended-chain $C_{246}H_{494}$ (see phase diagram, Figure 8).

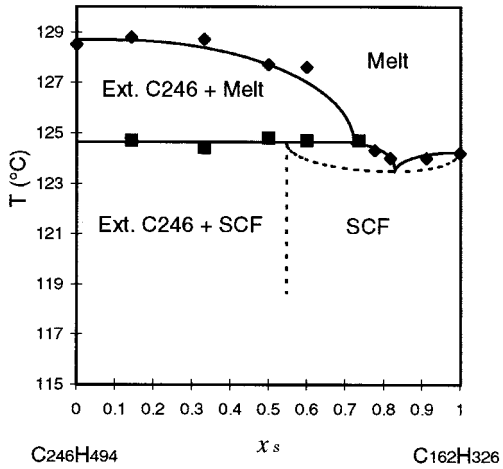

Figure 8. Equilibrium phase diagram of the $C_{162}H_{326}$ + $C_{246}H_{494}$ binary system. x_s = molar fraction of $C_{162}H_{326}$.

We note that in real-time SAXS experiments on isothermal crystallization of certain other $C_{162}H_{326}$ + $C_{246}H_{494}$ mixtures a semicrystalline phase with folded $C_{246}H_{494}$ chains is seen to form transiently at first. Soon an abrupt jump in ℓ_c to the value characteristic of extended $C_{162}H_{326}$ chains follows. Details of these experiments will be reported separately.[43]

3.2. Phase Diagram. Having established the likely lamellar structure of the full range of $C_{162}H_{326}$ + $C_{246}H_{494}$ alkane mixtures, we proceed to construct the phase diagram for this binary system. Eight mixtures of $C_{162}H_{326}$ and $C_{246}H_{494}$ were prepared, with the component ratios 10:90, 25:75, 40:60, 50:50, 65:35, 70:30, 75:25, and 88:12 by weight. Their crystallization and melting behavior, together with those of pure $C_{162}H_{326}$ and $C_{246}H_{494}$, were then examined by DSC and SAXS. Transition temperatures and enthalpies were found to be in good agreement with our structure assignment by X-ray diffraction.

The binary equilibrium phase diagram of $C_{162}H_{326}$ and $C_{246}H_{494}$ is constructed as shown in Figure 8. Above the triple temperature (124.7 ± 0.3 °C) the system is described by a simple crystal-solvent equilibrium, crystal being extended-chain $C_{246}H_{494}$ and solvent being molten $C_{162}H_{326}$. The three-phase line is caused by the changeover to an equilibrium between SCF and molten $C_{162}H_{326}$. This equilibrium is characterized by an almost horizontal liquidus with a shallow minimum around 0.85 molar $C_{162}H_{326}$. For the discussion in the next section it is important to establish the phase boundaries of the semicrystalline phase. At temperatures below the

Table 2. Determination of the SCF/SCF + $C_{246}H_{494}$ Phase Boundary

overall weight ratio $C_{162}H_{326}$:$C_{246}H_{494}$ in mixture	ΔH_f[a] (J/g)	W_{C246}[b]	x_s[c]
10:90	249	0.12	0.56
25:75	232	0.32	0.54
40:60	224	0.41	0.59
pure $C_{246}H_{494}$	260		

[a] Combined heat of fusion $\Delta H_{f\,SCF} + \Delta H_{f\,C246extd}$. [b] Weight fraction of the total $C_{246}H_{494}$ which is contained within SCF: $W_{C246} = (\Delta H_{f\,C246} - \Delta H_{f\,mixture})/\Delta H_{f\,C246}$*246/(246−162). [c] Molar fraction of $C_{162}H_{326}$ (x_s) in SCF.

triple point we find the single phase SCF to be stable in the range $0.56 \pm 0.04 < x_s < 1$, where x_s is the molar fractions of $C_{162}H_{326}$.

Three mixtures of $C_{162}H_{326}$ and $C_{246}H_{494}$ (10:90, 25:75, and 40:60 by weight) were closely examined to establish the boundary between single phase SCF and the biphasic region (extended $C_{246}H_{494}$ crystal + SCF), i.e., the minimum mole fraction of $C_{162}H_{326}$ (x_s) in SCF. Samples were brought quickly (50 °C/min) from melt to 121 °C, thus avoiding any growth of $C_{246}H_{494}$ in the extended chain form on the way, and then kept isothermally for several hours. Two endotherms were observed in the subsequent heating scan corresponding, respectively, to melting of SCF and of extended $C_{246}H_{494}$. Since it was uncertain as to what fraction of the second peak corresponded to material recrystallized during the heating scan, the total heat of fusion ΔH_f combining the two endotherms was measured. For the three mixtures, the ΔH_f values are given in Table 2. With the pure extended chain form as the reference (260 J/g, Table 2), the weight fraction of $C_{246}H_{494}$ molecules (W_{C246}) whose tails stayed in the amorphous state, hence in the SCF form, was calculated for each mixture. The minimum molar fraction of $C_{162}H_{326}$ in SCF is thus determined as $x_s = 0.56 \pm 0.04$. The upper limit, i.e., the maximum molar fraction, appears to be 1; there is no clear discontinuity between SCF and pure extended-chain $C_{162}H_{326}$ with changing composition.

3.3. Thermodynamic Analysis. From the phase diagram constructed for $C_{246}H_{494}$ and $C_{162}H_{326}$ mixture, it is evident that the semicrystalline form can be a stable phase of a binary mixture of two disparate long-chain paraffins. It may seem surprising that the system should choose a low crystallinity state in preference to a fully crystalline state, albeit a phase separated one. As shown above, the degree of crystallinity of SCF in the 1:1 w/w $C_{162}H_{326}$ + $C_{246}H_{494}$ mixture is only 0.8, becoming as low as 0.6 in the 1:1 molar mixture of $C_{122}H_{246}$ and $C_{210}H_{422}$. In this section, we carry out a simple thermodynamic analysis of SCF based on its structural model in order to understand the reason for its stability.

3.3.1. Phase-Separated Extended Chain Crystal. The molar free energy of a crystalline *n*-alkane in the extended chain form consists of the free energy of CH_2 units and a contribution from chain ends:[44]

$$\mu_s^c = n_s(h^c - Ts^c) + 2\sigma_e \quad (6a)$$

$$\mu_l^c = n_l(h^c - Ts^c) + 2\sigma_e \quad (6b)$$

h^c and s^c are, respectively, the molar enthalpy and entropy of CH_2 groups in the extended chain form, n the number of carbon atoms in the molecular chain, and $2\sigma_e$ is the surface free energy. Subscripts s and l denote the shorter and the longer chain alkane. In a phase separated crystalline mixture there is no interaction between the components, hence the free energy of the system is

$$\mu^c = x_s^c\mu_s^c + x_l^c\mu_l^c = (x_s n_s + x_l n_l)(h^c - Ts^c) + 2\sigma_e \quad (7)$$

where x is the molar fraction of the component in the binary mixture.

3.3.2. Semicrystalline Form. In the SCF, the states of the two molecular species are rather different according to our model, so their chemical potential must be dealt with separately. The shorter molecules are fully crystalline and confined to the crystalline layer. Their chemical potential can be expressed as

$$\mu_s^{SCF} = n_s(h^c - Ts^c) + 2\sigma_e + RT \ln x_s + \mu_s^i(x_s) \quad (8a)$$

The first two terms are the same as those for the extended chain form in the pure *n*-alkane. $RT \ln x_s$ comes from the entropy of mixing in the crystalline layer where the molecules of the two species can exchange positions. $\mu_s^i(x_s)$ is an additional term which takes into account the change in the environment of chain ends due to the presence of amorphous cilia; this term is examined further below.

The longer molecules are only partially crystalline with the cilia outside the crystalline layer. We shall treat the cilia as melt. Thus, the chemical potential of the longer molecules is

$$\mu_l^{SCF} = n_s(h^c - Ts^c) + (n_l - n_s)(h^m - Ts^m) - RT \ln(n_l - n_s) + RT \ln x_l + \mu_l^i(x_l) \quad (8b)$$

The first term is the free energy of the crystalline part and the second term that of the amorphous part. $RT \ln(n_l - n_s)$ comes from the additional choice of position of a molecule, i.e., from its ability to slide up and down through the crystalline layer as long as it keeps n_s number of CH_2 segments within the layer.

Thus, the molar free energy of the semicrystalline form is

$$\mu^{SCF} = x_s\mu_s^{SCF} + x_l\mu_l^{SCF} = n_s(h^c - Ts^c) + 2x_s\sigma_e + x_l((n_l - n_s)(h^m - Ts^m) - RT \ln(n_l - n_s)) + RT(x_s \ln x_s + x_l \ln x_l) + \mu^i \quad (9)$$

where $\mu^i = x_s\mu_s^i(x_s) + x_l\mu_l^i(x_l)$. This term deals with the crystalline−amorphous interface and is dominated by the "overcrowding" effect. In the case of semicrystalline polyethylene it has long been recognized that the cross-sectional area required by an amorphous chain is at least twice that required by a straight crystalline chain (the "Gambler's Ruin" problem).[45−49] This results in overcrowding at the crystal surface. In polymers, this problem is usually resolved partly by chain tilt, a solution adopted also by melt-crystallized alkanes. For the greater part, however, overcrowding in polymers is overcome by adjacently re-entrant chain-folding. Turning to alkane mixtures, in the case of a mixture with low x_l, the overcrowding problem is resolved by the shorter chains ending at the crystal surface. However, for high x_l the problem becomes insoluble. A solution like that in polyethylene is not viable since a chain-folded crystal would be too thin to be stable.

The position of the SCF phase boundary in our phase diagram (Figure 8) indicates that the overcrowding problem becomes serious around $x_l = 0.44$. In our present simple treatment we can therefore approximate μ^i as being zero for x_l up to around 0.44 and infinity for x_l above that value. Since the chains in SCF are tilted by 35°, it follows that the effective cross-sectional area of a chain crossing the crystalline−amorphous interface increases by a factor of $(0.44 \cos 35°)^{-1} = 2.8$. This experimental value should be compared with those in the range of 2−3 obtained theoretically or by simulation (see above).

Note that we have omitted the surface free energy term $2\sigma_e$ from the expression for μ_l^{SCF} (eq 8b). While this may be an oversimplification, we believe that by far the largest part of the free energy of a chain crossing the crystal−amorphous interface is contained within μ^i. The excess energy due to broken van der Waals bonds is the main contributor to the $2\sigma_e$ term for chains ending at the interface. This should be significantly reduced for chains bridging the interface.

3.3.3. Comparison of Free Energies of SCF and Phase-Separated Extended-Chain Crystals. The difference between the free energy of SCF (eq 9) and of phase separated extended chain crystals (eq 7) equals

$$\begin{aligned}\mu^{SCF} - \mu^c &= x_l\{(n_l - n_s)[(h^m - Ts^m) - (h^c - Ts^c)] - RT \ln(n_l - n_s) - 2\sigma_e\} + RT(x_s \ln x_s + x_l \ln x_l) + \mu^i \\ &= x_l(n_l - n_s)(T_0 - T)\Delta s - x_l RT \ln(n_l - n_s) + RT(x_s \ln x_s + x_l \ln x_l) - 2x_l\sigma_e + \mu^i \quad (10)\end{aligned}$$

where $h^m - h^c = T_0\Delta s$ and $\Delta s = s^m - s^c$, T_0 is the equilbrium melting point of polyethylene and Δs is the entropy of fusion.

According to (10), compared to the phase-separated extended-chain crystal state, in the SCF the free energy is higher by $x_l(n_l - n_s)(T_0 - T)\Delta s$ (8.2 kJ·mol^{-1} for $C_{162}H_{326} + C_{246}H_{494}$, 1:1 w/w, at 390 K, $T_0 = 415$ K.[50]) due to uncrystallized cilia. At the same time the free energy is reduced by the entropy of mixing ($RT(x_s \ln x_s + x_l \ln x_l)$, −2.2 kJ·mol^{-1}) and the translational unfreezing of the longer molecules ($-x_l RT \ln(n_l - n_s)$, −5.5 kJ·mol^{-1}). We suggest that the small remaining surplus of 0.5 kJ·mol^{-1} is easily compensated for through lowering of end-surface free energy relative to that for extended chain crystals ($2\sigma_e = 12$ kJ·mol^{-1}),[50] as SCF allows surface roughness without chain-end overcrowding. As long as the extra free energy due to surface overcrowding (μ^i) remains small, which we believe to be true when the majority of the binary mixture is the shorter *n*-alkane, in a certain temperature region the mixed SCF is more stable than the phase-separated extended chain crystal.

In the following, we will establish more rigorously the conditions under which SCF can be the stable phase of the binary system. For an *n*-alkane with $n = n_l - n_s$, the free energy in the solid state is $(n_l - n_s)(h^c - Ts^c) + 2\sigma_e$, while in the melt it is $(n_l - n_s)(h^m - Ts^m) - RT \ln(n_l - n_s)$. At the melting point T^m_{l-s} we have

$$(n_l - n_s)(h^m - T^m_{l-s}s^m) - RT^m_{l-s}\ln(n_l - n_s) - (n_l - n_s)(h^c - T^m_{l-s}s^c) - 2\sigma_e = (n_l - n_s)(T_0 - T^m_{l-s})\Delta s - RT^m_{l-s}\ln(n_l - n_s) - 2\sigma_e = 0 \quad (11)$$

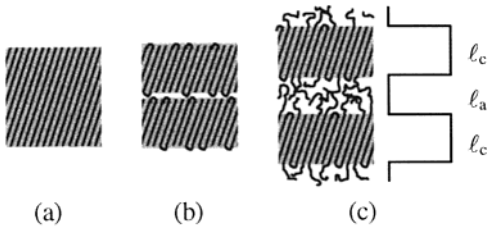

Figure 9. Schematic representation of molecular arrangement in different lamellar forms of pure long *n*-alkanes: (a) extended-chain form; (b) once-folded chain form; (c) noninteger folded (NIF) form.

Combining eqs 10 and 11 gives

$$\mu^{SCF} - \mu^c = -x_l(n_l - n_s)(T - T^m_{l-s})\Delta s - x_l R(T - T^m_{l-s}) \ln(n_l - n_s) + RT(x_s \ln x_s + x_l \ln x_l) + \mu^i \quad (12)$$

In the case of a $C_{162}H_{326}$−$C_{246}H_{494}$ mixture T^m_{l-s} is equal to the melting point of $C_{84}H_{170}$, which is 110 °C,[51] or 14 deg below that of the extended chain $C_{162}H_{326}$. Thus, in the temperature region bounded approximately by T^m_s and T^m_{l-s}, the free energy of SCF is lower than that of phase separated extended chain crystals as long as μ^i is small.

In summary, the following conditions need be satisfied for the semicrystalline (SCF) form to be the stable phase, in preference to the fully crystalline but phase separated extended chain forms:

1. The proportion of shorter molecules in the binary mixture must be sufficiently high to overcome overcrowding at the crystal−amorphous interface. In the case of the $C_{162}H_{326} + C_{246}H_{494}$ mixture, the present results show that the molar fraction of $C_{162}H_{326}$ must be above 0.56 for the semicrystalline form to be stable.
2. Temperature must be in the range delimited approximately by the melting point of shorter *n*-alkane and that of the $(n_l - n_s)$-alkane. In the $C_{162}H_{326}$−$C_{246}H_{494}$ system, this falls between approximately 124 and 110 °C, as indeed observed.

4. Discussion

SCF is unique as it is a thermodynamically stable semicrystalline phase made up of fully crystallizable components. Alternating crystalline and amorphous layer structures exist in semicrystalline polymers, but these are metastable and are the results of crystallization kinetics; annealing usually increase crystallinity and in favorable cases fully crystalline extended-chain morphology can be obtained.[52,53] On the other hand, semicrystalline structures can also be obtained in block copolymers where microphase separation can occur between a crystallizable and a noncrystallizable block[54] or between two crystallizable block at a temperature where one block is molten.[55] However, these copolymer systems have no alternative as full phase separation is prohibited by the bond between the blocks. To our knowledge, SCF in mixed long alkanes is the first example of a semicrystalline form being stable against an accessible fully crystalline state.

The structural model of SCF in mixed alkanes bears close resemblance to that of the noninteger folded (NIF) form in pure long chain *n*-alkanes (Figure 9). Both of these phases have a semicrystalline lamellar structure, except that NIF is metastable and transient, transforming isothermally into a highly crystalline form, either extended-chain or folded-chain,[11] or into a more complex

folded−extended crystalline form.[42] Although NIF consists of molecules of one and the same species, it contains two types of chains: some that are folded in half and fully crystalline, others that traverse the crystal layer only once with half their length remaining amorphous. Thus, ℓ_c in NIF corresponds to half the chain length, i.e., to the length of the fold.

Because of their different nature NIF and SCF behave differently on annealing. In the case of NIF, the amorphous thickness ℓ_a and the overall periodicity L decrease with time as the proportion of folded chains increases and the amorphous cilia disappear ("lamellar thinning").[12] On the other hand in the binary mixtures ℓ_a and L remain constant indefinitely. Furthermore, at higher annealing temperatures, within 6−7 °C below its melting point, NIF in pure alkanes transforms to the extended-chain form, the transformation being complete within 2−4 min in the case of $C_{246}H_{494}$[56] and less in $C_{198}H_{398}$.[57] In contrast, in the temperature and composition range of stability of SCF extended-chain crystals do not appear at all. This comparison with NIF suggests that there is sufficient mobility for the transformation of SCF into a more stable state if there was a driving force.

The 1:9 w/w mixture of $C_{162}H_{326}$ and $C_{246}H_{494}$ presents a case where NIF appears in a mixture. ℓ_c is set by the folded chains of $C_{246}H_{494}$ rather than by extended chains of $C_{162}H_{326}$—see Figure 6b. Here the amorphous sublayer must contain cilia coming from both $C_{162}H_{326}$ and $C_{246}H_{494}$. Assuming amorphous and crystalline densities to be 0.8 and 1.0, if all $C_{246}H_{494}$ chains were folded, ℓ_a would have been only 18 Å, as opposed to the 93 Å actually measured. Simple calculation shows that only 35% of the $C_{246}H_{494}$ is folded.[12]

The importance of cilia in the formation of polymer morphology has been highlighted by Bassett and coworkers;[58] splay of crystalline lamellae associated with spherulite formation has been attributed to repulsion of cilia due to the entropic elastic force. Lamellar branching and cellulation has been studied in spherulite-like morphology observed on crystallization of dilute blends of the above long alkanes at high supercooling.[59]

A comment is due regarding the comparison with shorter alkanes, i.e., those containing a few tens of C atoms. Here too binary mixtures were found in some cases to form stable solid solutions with a lamellar thickness intermediate between those of the extended forms of the components.[13] A Gaussian distribution of atom site occupancy at the chain ends was used to fit the experimental data.[13] Similar treatment was adopted in the single-crystal X-ray study of Gerson et al [15] on β-$C_{24}H_{50}$ + $C_{26}H_{54}$ and β_0-$C_{20}H_{42}$ + $C_{22}H_{46}$. In some respects this is similar to the SCF in long chain *n*-alkane mixtures. However, in mixtures of short alkanes the intercrystalline layers are normally confined to only several CH_2 groups at the surface, as the chain lengths of miscible components in shorter paraffins do not differ by more than a few carbons. It may therefore be more appropriate to describe these systems as having enhanced surface disorder. In contrast, the thickness of intercrystalline layers in mixtures of long alkanes can exceed a hundred angstroms with flat low density; there is compelling evidence that these intercrystalline layers are truly amorphous.

5. Conclusions

1. Binary mixtures of *n*-alkanes with carbon numbers in the range between 122 and 294 with a chain length ratio up to 2 were found to form solid solutions. These appear to be stable for chain lengths ratios up to 1.7 ($C_{122}H_{246}$ + $C_{210}H_{422}$), or a chain length difference up to 100 carbons between the components ($C_{194}H_{390}$ + $C_{294}H_{590}$).

2. The solid solution has a high-temperature and a low-temperature phase, separated by a first-order transition.

3. The high-temperature phase is semicrystalline (SCF) with a lamellar structure consisting of alternating crystalline and amorphous layers.

4. In SCF molecules of the shorter alkane are fully extended and confined to the crystalline layer; hence, their chain length determines the thickness of this layer. The molecules of the longer component traverse the crystalline layer, but their surplus length remains as amorphous cilia.

5. The binary phase diagram of a typical mixture, $C_{162}H_{326}$ + $C_{246}H_{494}$, shows that below the melting point of $C_{162}H_{326}$ SCF is the stable phase for $0.56 < x_s < 1$, where x_s is the molar fraction of $C_{162}H_{326}$.

6. In cases where the chain length and the proportion of the longer alkane are high (e.g., 1:9 $C_{162}H_{326}$ + $C_{246}H_{494}$) the thickness of the crystalline sublayer is determined by the fold length of the folded-chain long alkane rather than by the extended length of the shorter one. This structures are equivalent to the "noninteger folded" (NIF) form found in pure long alkanes and, like NIF, are metastable.

7. The volume crystallinity of stable SCF can be as low as 63% ($C_{122}H_{246}$ + $C_{210}H_{422}$), and even lower for metastable SCFs (56% in $C_{122}H_{246}$ + $C_{246}H_{494}$ and 54% in 1:9 $C_{162}H_{326}$ + $C_{246}H_{494}$).

8. A simple thermodynamic analysis based on the structure model of semicrystalline form shows the plausibility of SCF being stable against fully crystalline phase-separated extended-chain alkanes.

9. SCF with specified crystalline and amorphous layer thicknesses can be obtained with an appropriate choice of *n*-alkanes and their composition, as long as the conditions for stability of SCF given in 3.3.3 are satisfied.

Acknowledgment. We wish to thank Mr. A. Gleeson of Daresbury Laboratory for help with setting up the SAXS experiments and the Centre of Molecular Materials, University of Sheffield, for letting us use their DSC instrument. This study was supported by the Engineering and Physical Sciences Research Council and the donors of the Petroleum Research Fund, administered by the American Chemical Society.

References and Notes

(1) Preliminary announcement was published in: Zeng, X. B.; Ungar, G. *Phys. Rev. Lett.* **2001**, *86*, 4875−4878.
(2) Bidd, I.; Whiting, M. C. *J. Chem. Soc., Chem. Commun.* **1985**, 543−544.
(3) Bidd, I.; Holdup, D. W.; Whiting, M. C. *J. Chem. Soc., Perkin Trans.* **1987**, *1*, 2455−2463.
(4) Lee, K. S.; Wegner, G. *Makromol. Chem., Rapid Commun.* **1985**, *6*, 203−208.
(5) Smith, A. E. *J. Chem. Phys.* **1953**, *21*, 2229−2231.
(6) Shearer, H. M. M.; Vand, V. *Acta Crystallogr.* **1956**, *9*, 379−384.
(7) Pieszek, W.; Strobl, G. R.; Makahn, K. *Acta Crystallogr.* **1974**, *B30*, 1278−1288.
(8) Ungar, G.; Stejny, J.; Keller, A.; Bidd, I.; Whiting, M. C. *Science* **1985**, *229*, 386-389.
(9) Organ, S. J.; Keller, A. *J. Polym. Sci. Polym. Phys. Ed.* **1987**, *25*, 2409−2430.

(10) Ungar, G.; Organ, S. J.; Keller, A. *J. Polym. Sci. Polym. Lett.* **1988**, *26*, 259−262.
(11) Ungar, G.; Keller, A. *Polymer* **1986**, *27*, 1835−1844.
(12) Zeng, X. B.; Ungar, G. *Polymer* **1998**, *19*, 4523−4533.
(13) Dorset, D. L. *Macromolecules* **1985**, *18*, 2158−2163; **1986**, *19*, 2965−2973; **1987**, *20*, 2782−2788; **1990**, *23*, 623−633.
(14) Snyder, R. G.; Conti, G.; Strauss, H. L.; Dorset, D. L. *J. Phys. Chem.* **1993**, *97*, 7342−7350.
(15) Gerson, A. R.; Nyburg, S. C. *Acta Crystallogr.* **1994**, *B50*, 252−256.
(16) Annis, B. K.; Londono, J. D.; Wignall, G. D.; Snyder, R. G. *J. Phys. Chem.* **1996**, *100*, 1725−1730.
(17) Dorset, D. L.; Snyder, R. G. *J. Phys. Chem.* **1996**, *100*, 9848−9853.
(18) Clavell_Grunbaum, D.; Strauss, H. L.; Snyder, R. G. *J. Phys. Chem.* **1997**, *B101*, 335−343.
(19) Dorset, D. L. *J. Phys. Chem.* **1997**, *B101*, 4870−4874.
(20) Gilbert, E. P. *Phys. Chem. Chem. Phys.* **1999**, *1*, 1517−1529; 2715−2724; 5209−5214.
(21) Sirota, E. B.; Herhold, A. B. *Science* **1999**, *283*, 529−532.
(22) Piper, S. H.; Chibnall, A. C.; Hopkins, S. J.; Pollard, A.; Smith, J. A. B.; Williams, E. F. *Biochem. J.* **1931**, *25*, 2072.
(23) Mazee, W. M. *Anal. Chim. Acta* **1957**, *17*, 97−106.
(24) Smith, A. E. *Acta Crystallogr.* **1957**, *10*, 802−803.
(25) Mnyukh, Yu. V. *J. Struct. Chem.* **1960**, *1*, 370−388.
(26) Nechitailo, N. A.; Topchier, A. V.; Rozenberg, L. M.; Terent'eva, E. M. *Russ. J. Phys. Chem.* **1960**, *34*, 1268−1272.
(27) Luth, H.; Nyburg, S. C.; Robingson, P. M.; Scott., H. G. *Mol. Cryst. Liq. Cryst.* **1974**, *27*, 337−357.
(28) Bonsor, D. H.; Bloor, D. *J. Mater. Sci.* **1977**, *12*, 1559−1564.
(29) Asbach, G. I.; Geiger, K.; Wilke, W. *Colloid Polym. Sci.* **1979**, *257*, 1049.
(30) Denicolo, I.; Craievich, A. F.; Doucet, J. *J. Chem. Phys.* **1984**, *80*, 6200−6203.
(31) Mondieig, D.; Espeau, P.; Robles, L.; Oonk, H. A. J.; Cuevas-Diarte, M. A. *J. Chem. Soc., Faraday Trans.* **1997**, *93*, 3343−3346.
(32) Gerson, A. R.; Nyburg, S. C.; McAleer, A. *J. Appl. Crystallogr.* **1999**, *32*, 296−299.
(33) Smith, P.; Manley, St. J. R. *Macromolecules* **1979**, *12*, 483−491.
(34) Brooke, G. M.; Burnett, S.; Mohammed, S.; Proctor, D.; Whiting, M. C. *J. Chem. Soc., Perkin Trans. 1* **1996**, 1635−1645.
(35) Zerbi, G.; Magni, R.; Gussoni, M.; Holland-Moritz, K.; Bigotto, A.; Dirlikov, S. *J. Chem. Phys.* **1981**, *75*, 3175−3194.
(36) Hohne, G. W. H.; Hemminger, W.; Flammersheim, H.-J. *Differential Scanning Calorimetry, An introduction for practitioners*, Springer: London, 1996.
(37) Bunn, C. W. *Trans. Faraday Soc.* **1939**, *35*, 483−491.
(38) Zeng, X. B.; Ungar, G. Manuscript in preparation.
(39) Boda, E.; Ungar, G.; Brooke, G. M.; Burnett, S.; Mohammed, S.; Proctor, D.; Whiting, M. C. *Macromolecules* **1997**, *30*, 4674−4678.
(40) Hoffman, J. D.; Davis, G. T.; Laurizen, J. I. Jr. In *Treatise in Solid State Chemistry*; Hannay, N. B., Eds.; Plenum: New York, 1976; p 497.
(41) Keller, A.; Goldbeck-Wood, G. *Comprehensive Polymer Science*, Second Suppl.; Allen, G., et al., Eds.; Pergamon: Oxford, England, 1996; p 241.
(42) Zeng, X. B.; Ungar, G.; Spells, S. J. *Polymer* **2000**, *41*, 8775−8780.
(43) Zeng, X. B.; Ungar, G. Manuscript in preparation.
(44) Flory, P. J.; Vrij, A. *J. Am. Chem. Soc.* **1963**, *85*, 3548−3553.
(45) Frank, F. C. *Discuss. Faraday Soc.* **1979**, *68*, 7−13.
(46) DiMarzio, E. A.; Guttman, C. M. *Polymer* **1980**, *21*, 733−744.
(47) Guttman, C. M.; DiMarzio, E. A.; Hoffman, J. D. *Polymer* **1981**, *22*, 1466−1479.
(48) Mansfield, M. L. *Macromolecules* **1988**, *21*, 126−130.
(49) Balijepalli, S.; Rutledge, G. C. *J. Chem. Phys.* **1998**, *109*, 6523−6526; *Macromol. Symp.* **1998**, *133*, 71−99.
(50) Wunderlich, B.; Czoenyi, G. *Macromolecules* **1977**, *10*, 906−913.
(51) Takamizawa, K.; Ogawa, Y.; Oyama, T. O. *Polym. J.* **1982**, *14*, 441−456.
(52) Wunderlich, B.; Arakawa, T. *J. Polym. Sci.* **1964**, *A2*, 3697.
(53) Bassett, D. C.; Turner, B. *Nature Phys. Sci.* **1972**, *240*, 146−148.
(54) Zhu, L.; Chen, Y.; Zhang, A. Q.; Calhoun, B. H.; Chun, M. S.; Quirk, R. P.; Cheng, S. Z. D.; Hsiao, B. S.; Yeh, F. J.; Hashimoto, T. *Phys. Rev.* **1999**, *B60*, 10022−10031.
(55) Mai, S. M.; Fairclough, J. P. A.; Viras, K. *Macromolecules* **1997**, *30*, 8392−8400.
(56) Ungar, G.; Keller, A. *Polymer* **1987**, *28*, 1899−1907.
(57) Ungar, G. Unpublished work.
(58) Bassett, D. C. *Macromol. Symp.* **1997**, *114*, 121−126. Bassett, D. C.; Olley, R. H.; Sutton, S. J.; Vaughan, A. S. *Polymer* **1996**, *37*, 4993−4997.
(59) Hosier, I. L.; Bassett, D. C.; Vaughan, A. S. *Macromolecules* **2000**, *33*, 8781−8790.

MA010853R